ECS Journal of Solid State Science and Technology, **7** (10) P519-P523 (2018)
2162-8769/2018/7(10)/P519/5/$37.00 © The Electrochemical Society

Band Offsets for Atomic Layer Deposited $HfSiO_4$ on $(Al_{0.14}Ga_{0.86})_2O_3$

Chaker Fares,[1] F. Ren,[1,*] Eric Lambers,[2] David C. Hays,[2] B. P. Gila,[2,3,] and S. J. Pearton[3,*,z]**

[1]*Department of Chemical Engineering, University of Florida, Gainesville, Florida 32611, USA*
[2]*Nanoscale Research Facility, University of Florida, Gainesville, Florida 32611, USA*
[3]*Department of Materials Science and Engineering, University of Florida, Gainesville, Florida 32611, USA*

There is increasing interest in $(Al_xGa_{1-x})_2O_3/Ga_2O_3$ metal-oxide semiconductor field effect transistors, but there is little information on appropriate gate dielectrics for the $(Al_xGa_{1-x})_2O_3$. A potential candidate is $HfSiO_4$ deposited by Atomic Layer Deposition (ALD), which should mitigate disruption to the surface. The valence band offset of the $HfSiO_4/(Al_{0.14}Ga_{0.86})_2O_3$ heterointerface was measured using X-Ray Photoelectron Spectroscopy. The single-crystal β-$(Al_{0.14}Ga_{0.86})_2O_3$ was grown by Molecular Beam Epitaxy. The bandgap of the $HfSiO_4$ was determined by Reflection Electron Energy Loss Spectroscopy to be 7.0 ± 0.35 eV, while high resolution XPS data of the O 1s peak and onset of elastic losses was used to establish the $(Al_{0.14}Ga_{0.86})_2O_3$ bandgap as 5.0 ± 0.30 eV. The valence band offset was 0.42 eV ± 0.10 eV (straddling gap, type I alignment) for ALD $HfSiO_4$ on β-$(Al_{0.14}Ga_{0.86})_2O_3$. The conduction band offset was 1.58 ± 0.35 eV, providing good electron confinement.
© 2018 The Electrochemical Society. [DOI: 10.1149/2.0041810jss]

Manuscript submitted August 20, 2018; revised manuscript received September 7, 2018. Published September 15, 2018.

β-Ga_2O_3 is attracting attention for power switching device applications as well as solar blind UV detection.[1–15] The β polymorph is the most prominent of the five phases of Ga_2O_3 and has a wide bandgap of ∼4.8 eV, a theoretical breakdown field of ∼8 $MV.cm^{-1}$ that is higher than either SiC or GaN and the ability to operate at temperatures in excess of 250°C.[1–3,8] The monoclinic crystal structure with space group C2/m consists of double octahedral chains, running parallel to the crystallographic y-axis,[2–4] as shown in Figure 1(top). The chains are cross-linked by tetrahedral GaO_4 groups. The beta phase is more stable at ambient conditions, but under heating it transforms to the alpha phase, which has the corundum (alumina) structure.[2–4] Most of the devices reported to date have employed pure Ga_2O_3, but there is strong interest in heterostructures involving β-$(Al,Ga)_2O_3$ monoclinic phase alloys.[15–19] In this system, the bandgap can be varied from 4.8–6 eV, providing the ability to make a variety of advanced devices based on β-$(Al_xGa_{1-x})_2O_3$/ Ga_2O_3 heterostructures. There are already device demonstrations of modulation-doped transistors in this materials system with impressive characteristics.[15–20]

The use of metal-oxide-semiconductor field-effect transistor (MOSFET) structures, combined with the advantages of heterostructures provides lower leakage currents and power consumption and capability for greater voltage swings relative to the more common Schottky-gate devices.[6,21] These larger gate voltage swings have the potential for operation in either enhancement mode or depletion mode. The development of gate dielectrics for $(Al_xGa_{1-x})_2O_3$ alloys is still in its infancy, but there are some general rules of thumb in materials selection. It is commonly accepted that a 1 eV bandgap difference between the gate insulator and the semiconductor is preferred for obtaining sufficient energy barrier to hole and electron leakage current.[2–6,22] To date, the most common dielectrics employed on Ga_2O_3 and related alloys have typically been Al_2O_3, HfO_2 or SiO_2.[23–36] To benefit from the large dielectric constant of HfO_2 and the wide bandgap of SiO_2, alternating layers of these dielectrics are often deposited to form $HfSiO_4$. $HfSiO_4$ is of particular interest due to its dielectric constant being significantly larger than SiO_2. The larger dielectric constant allows for an equivalent capacitance in thicker films which is advantageous in MOS device applications. Additionally, by altering the HfO_2:SiO_2 ratio, the bandgap and dielectric constant can be tuned for $Hf_{1-x}Si_xO_4$.

The valence band offset is normally measured directly using X-Ray Photoelectron Spectroscopy (XPS) and the conduction band offset is then calculated from the difference between that and the bandgaps of the dielectric and semiconductor.[36–39] Atomic Layer Deposition (ALD) is an attractive option because it provides minimal disruption to the heterointerface and can be used with a remote plasma to reduce the effects of contamination.

In this paper, we report on the determination of the band alignment in the $HfSiO_4/(Al_{0.14}Ga_{0.86})_2O_3$ heterostructure, in which the $HfSiO_2$ was deposited by ALD onto $(Al_{0.14}Ga_{0.86})_2O_3$ grown by Molecular Beam Epitaxy (MBE). The valence band offset was obtained from XPS measurements and by measuring the respective bandgaps of the $HfSiO_4$ (7.0 ± 0.35 eV) and β-$(Al_{0.14}Ga_{0.86})_2O_3$ (5.0 ± 0.30 eV), we were able to determine both the conduction band offset in the heterostructures and determine the band alignment type.

Experimental

Alternating cycles of HfO_2 and SiO_2 were grown by ALD on $(Al_{0.14}Ga_{0.86})_2O_3/Ga_2O_3$ structures and quartz substrates to form a ternary film with the composition of $HfSiO_4$.[35] The latter were used for dielectric constant and composition measurements. Both thick (150 nm) and thin (1.5 nm) layers of the dielectrics were deposited

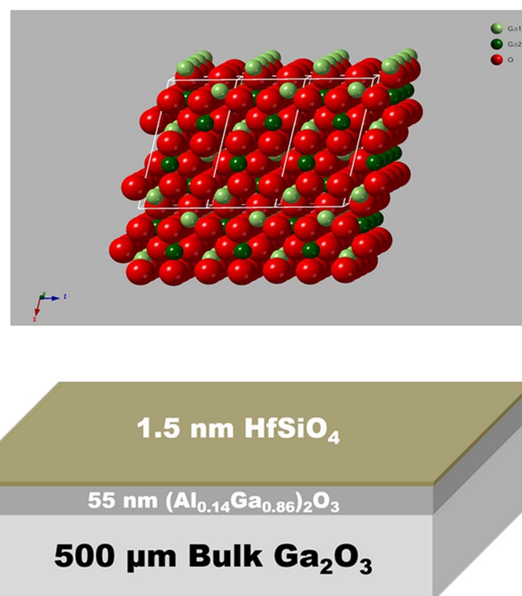

Figure 1. Schematic of β-Ga_2O_3 lattice structure (top) and composition and corresponding thicknesses of layer structure used (bottom).

*Electrochemical Society Fellow.
**Electrochemical Society Member.
[z]E-mail: spear@mse.ufl.edu

Downloaded on 2018-10-30 to IP 128.227.118.70 address. Redistribution subject to ECS terms of use (see ecsdl.org/site/terms_use) unless CC License in place (see abstract).

to be able to measure both bandgaps and core levels on the β-$(Al_{0.14}Ga_{0.86})_2O_3$. For substrate cleaning pre-deposition, the following rinse sequence was employed: acetone, IPA, N_2 dry and finally Ozone exposure for 15 min. The $HfSiO_4$ layers were deposited at 200°C in a Cambridge Nano Fiji 200, a remote plasma atomic layer deposition tool, using an ICP source at 300 W. Plasma mode ALD helps lower contaminants in the film and reduces the nucleation delay while minimizing ion induced damage by utilizing a remote source. The sequence of dielectric deposition started with HfO_2 being deposited first using precursors of Tetrakis (dimethylamido) hafnium (IV) and O_2 at a deposition rate of 0.9 A/cycle.[35] Likewise, the SiO_2 layers were deposited using precursors of Tris (dimethylamino) silane and O_2, and produced a deposition rate of 0.6 A/cycle[35] To achieve an atomic concentration of $Hf_{0.5}Si_{0.5}O_4$, three SiO_2 cycles (1.8 A) were followed by two HfO_2 cycles (1.8 A) to keep a 1:1 ratio. A previous study reported no difference in the starting layer (SiO_2 or HfO_2) on band offset[35] although published theoretical work states even one monolayer can be enough to alter band alignment contingent on intralayer electronegativity.[40–46] These films were deposited onto epi $(Al_{0.14}Ga_{0.86})_2O_3$ that was grown by Molecular Beam Epitaxy. These AGO layers were doped with Si to produce an n-type carrier density of 10^{17} cm^{-3} and were 55 nm thick. The carrier concentration was determined by electrochemical capacitance-voltage (ECV) profiling at a frequency of 740 Hz on calibration samples and the composition was determined by X-ray diffraction on these same samples. These epitaxial layers were grown on top of Sn-doped (6.3×10^{18} cm^{-3}) bulk β-phase Ga_2O_3 single crystal substrates (500 μm thick) with (010) surface orientation (Tamura Corporation, Japan) grown by the edge-defined film-fed growth method. The heterostructure sample is shown schematically in Figure 1(bottom).

XPS survey scans were used to obtain the chemical state of the $HfSiO_4$ and β-$(Al_{0.14}Ga_{0.86})_2O_3$ and identify peaks for high resolution analysis.[37] An ULVAC PHI XPS with a monochromatic, micro-focused, aluminum X-ray source (energy 1486.6 eV) at a source power of 300 W was used. The analysis area was 10 μm in diameter while a take-off angle of 50° and an acceptance angle of ± 7 degrees were utilized. The electron pass energy was 23.5 eV for the high-resolution scans and 93.5 eV for the survey scans. The approximate escape depth (3λ sin θ) of the electrons was 80 Å. In this system, all of the peaks are well-defined.

Charge compensation was performed using a dual beam charge neutralization system. This system utilizes a low-energy electron beam and ion beam simultaneously to prevent charge buildup during data collection.[36] The charge neutralization system is often not sufficient at eliminating all surface charge, and additional corrections must be performed. Using the known position of the adventitious carbon (C-C) line in the C 1s spectra at 284.8 eV, charge correction was performed. During the measurements, the samples and electron analyzers were electrically grounded to provide a common reference Fermi level. Differential charging is a concern for semiconductor band offset measurements[41–48] and while use of an electron flood gun does not guarantee that differential charging is not present, our experience with oxides on conducting substrates has been that the differential charging is minimized with the use of an electron gun. Calibrations with and without the gun and verified that was the case. This procedure has been described in detail previously.[36]

Reflection electron energy loss spectroscopy (REELS) was employed to measure the bandgap of the $HfSiO_4$.[39,40] By taking a linear fit to the leading plasmon peak and finding its zero energy with the background, a direct measurement of valence to conduction band energy is made. REELS spectra were obtained using a 1 kV electron beam and the hemispherical electron analyzer.

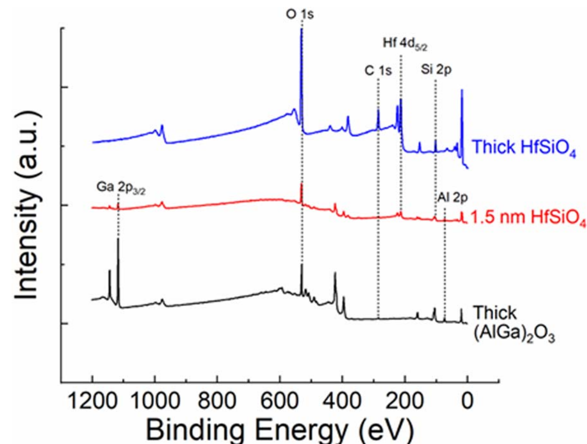

Figure 2. XPS survey scans of thick ALD $HfSiO_4$, 1.5 nm ALD $HfSiO_4$ on $(Al_{0.14}Ga_{0.86})_2O_3$, and $(Al_{0.14}Ga_{0.86})_2O_3$ reference sample. The intensity is in arbitrary units (a.u.).

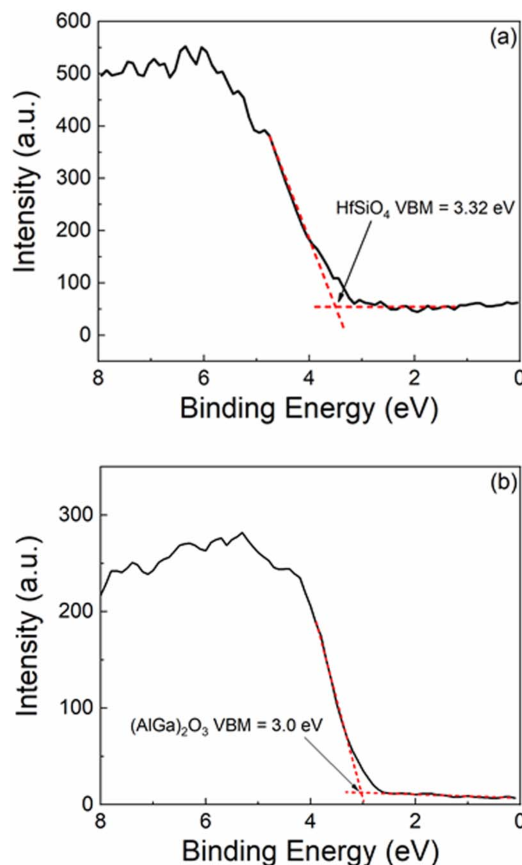

Figure 3. XPS spectra of core levels to valence band maximum (VBM) for (a) thick film $HfSiO_4$ deposited by ALD and (b) reference $(Al_{0.14}Ga_{0.86})_2O_3$. The intensity is in arbitrary units (a.u.).

Results and Discussion

Figure 2 shows the stacked XPS survey scans of thick (200 nm) $HfSiO_4$, 1.5 nm ALD $HfSiO_4$ on β-$(Al_{0.14}Ga_{0.86})_2O_3$, and an $(Al_{0.14}Ga_{0.86})_2O_3$ reference sample. The spectra show only the lattice constituents are present to the sensitivity of the measurement from contaminants. By contrast, in sputtered films it has been reported that metallic contaminants can form oxides that reduce the overall bandgap of the dielectrics and affect the resulting band alignment derived from the data.[41–43]

The valence band maximum (VBM) was determined by linearly fitting the leading edge of the valence band and the flat energy distribution from the XPS measurements, and finding the intersection of these two lines,[37,38] as shown in Figure 3 for the thick $HfSiO_4$, and

Downloaded on 2018-10-30 to IP 128.227.118.70 address. Redistribution subject to ECS terms of use (see ecsdl.org/site/terms_use) unless CC License in place (see abstract).

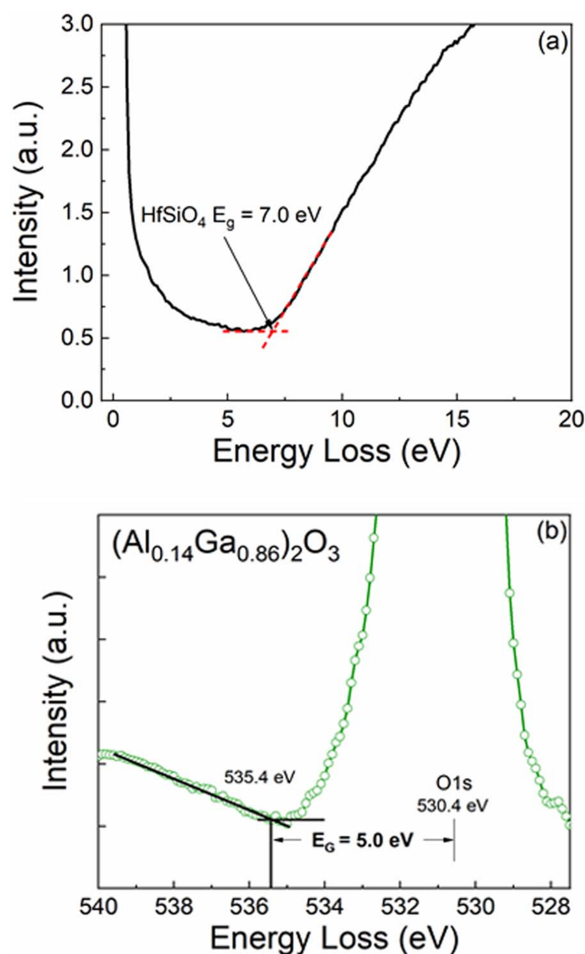

Figure 4. Bandgap of (a) $HfSiO_4$ and (b) $(Al_{0.14}Ga_{0.86})_2O_3$ determined by Reflection Electron Energy Loss Spectra and the onset of energy loss spectrum, respectively. The intensities are in arbitrary units (a.u.).

the $(Al_{0.14}Ga_{0.86})_2O_3$. The VBMs were measured to be 3.0 ± 0.2 eV for β-$(Al_{0.14}Ga_{0.86})_2O_3$ and 3.32 ± 0.4 eV for the $HfSiO_4$.

The measured bandgap for the $HfSiO_4$ was 7.0 ± 0.35 eV from the REELS data of Figure 4a. The bandgap of the β-$(Al_{0.14}Ga_{0.86})_2O_3$ was determined to be 5.0 ± 0.3 eV, from XPS O1s based electron energy loss measurements which is shown in Figure 4b.[39] The difference in bandgaps between $HfSiO_4$ and β-Ga_2O_3 is therefore 2.0 eV. This is consistent with past work on powdered samples of $(Al_xGa_{1-x})_2O_3$ over the composition range x = 0 - 0.4.[44] Using that linear relationship for bandgap as a function of composition leads to an expected value of 5.01 eV for x = 0.14, consistent with our data. Others have[21] reported a more pronounced bowing behavior for the compositional dependence of bandgap in $(Al_xGa_{1-x})_2O_3$ alloys, with systematically lower bandgaps at each composition, including pure Ga_2O_3, but they indicated there was significant strain in their films which would alter the result. If we use the theoretical relationship derived by Peelaers et al.,[22] we would expect a bandgap of 5.14 eV for our sample with x = 0.14, close to our experimental result.

The band alignment and valence and conduction band offsets were obtained from the examined the core level spectra using the now-standard method due to Kraut et al.[37] This method relies on precise measurement of a core level and the valence band edge for each material investigated and measurement in the shift of the core levels when the two materials have formed the heterojunction. The equation used to calculate the offset is:

$$\Delta E_V = \left(E^1_{core} - E^1_{VBM}\right) - \left(E^2_{core} - E^2_{VBM}\right) - \left(E^1_{core} - E^2_{core}\right)$$

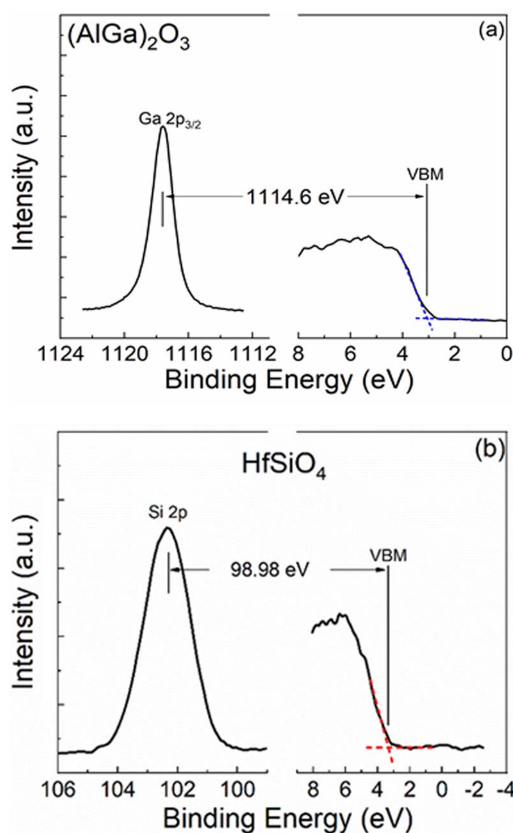

Figure 5. High resolution XPS spectra for the vacuum-core delta regions of (a) bulk $(Al_{0.14}Ga_{0.86})_2O_3$ and (b) ALD $HfSiO_4$. The intensity is in arbitrary units (a.u.).

It is important to use a well-defined core level since the offsets are small compared to the core level energy and more deviation is expected at higher core level energies.

High resolution XPS spectra of the VBM-core delta region are shown in Figure 5a for the β-$(Al_{0.14}Ga_{0.86})_2O_3$ and thick ALD $HfSiO_4$ Figure 5b samples. These were used to determine the selected core level peak positions. Figure 6 shows the XPS spectra for the β-$(Al_{0.14}Ga_{0.86})_2O_3$ to $HfSiO_4$ core delta regions of the heterostructure samples. These values are summarized in Table I and were then used to calculate ΔEv.

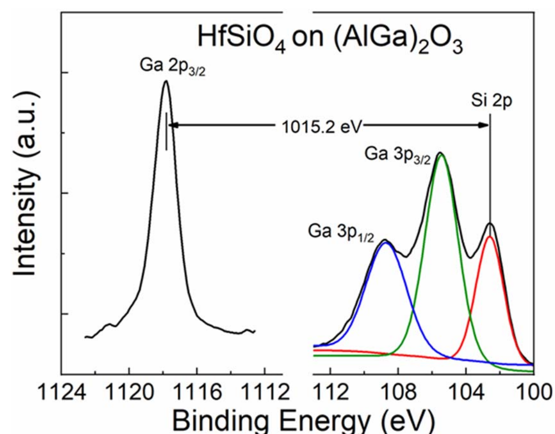

Figure 6. High resolution XPS spectra for the $(Al_{0.14}Ga)_2O_3$ to $HfSiO_4$ core delta regions. The intensity is in arbitrary units (a.u.).

Downloaded on 2018-10-30 to IP 128.227.118.70 address. Redistribution subject to ECS terms of use (see ecsdl.org/site/terms_use) unless CC License in place (see abstract).

Table I. Summary of measured core levels in these experiments (eV).

Reference $(AlGa)_2O_3$				Reference $HfSiO_4$				Thin $HfSiO_4$ on $(AlGa)_2O_3$	
Core Level	VBM	Core Level Peak	Core - VBM	Core Level	VBM	Core Level Peak	Core - VBM	Δ Core Level Ga $2p_{3/2}$ - Si 2p	Valence Band Offset
Ga$2p_{3/2}$	3.00	1117.60	1114.60	Si 2p	3.32	102.30	98.98	1015.20	0.42

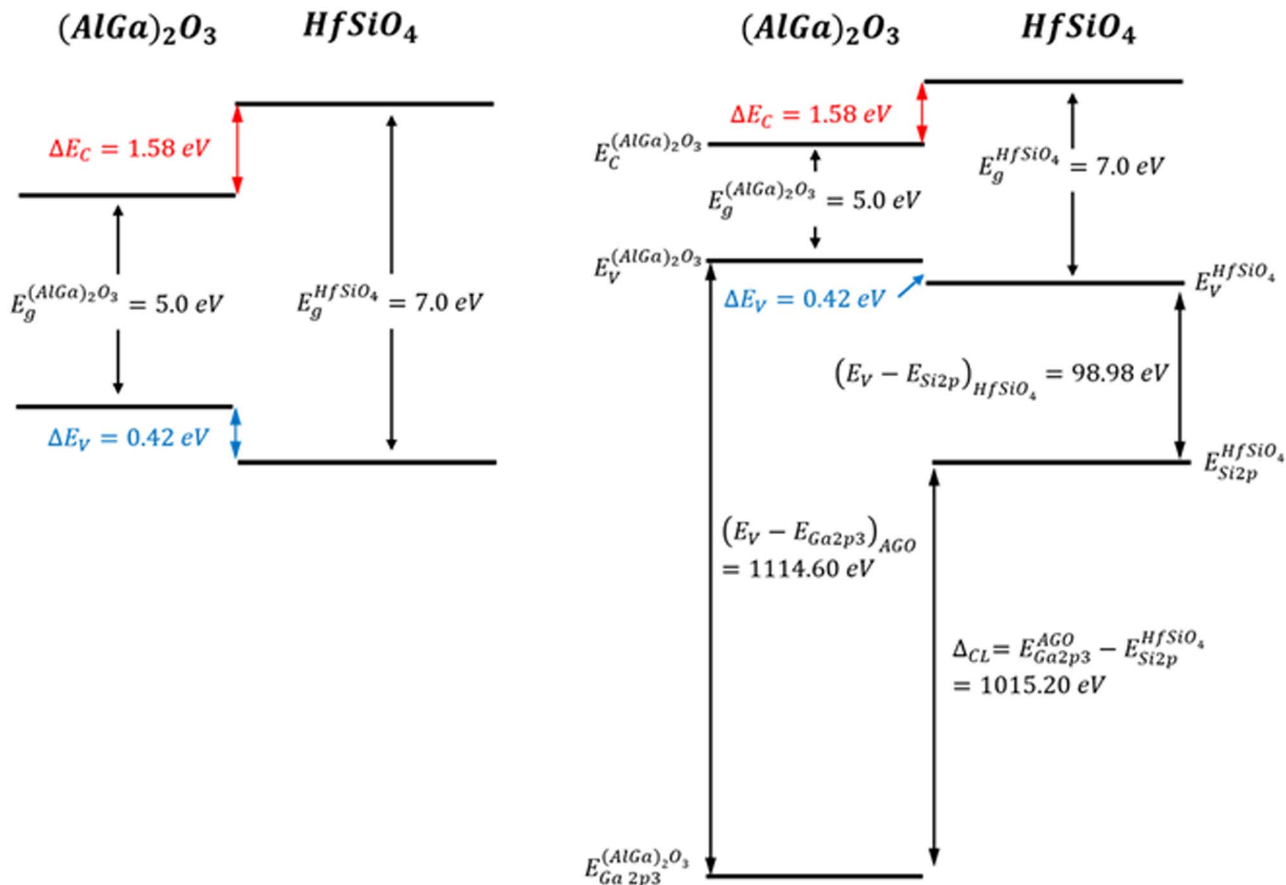

Figure 7. Summary (left) and detailed (right) band diagrams for the $HfSiO_4/(Al_{0.14}Ga_{0.86})_2O_3$ heterostructure in which the $HfSiO_4$ was deposited by ALD. The valence band offset was determined to be 0.42 eV ± 0.10 eV for ALD $HfSiO_4$ on β-$(Al_{0.14}Ga_{0.86})_2O_3$. The conduction band offset was 1.58 ± 0.35 eV.

Figure 7 shows the band alignment of the $HfSiO_4$/β-$(Al_{0.14}Ga_{0.86})_2O_3$ heterostructure. This is a nested, type I system with a valence band offset of 0.42 ± 0.10 eV and conduction band offset of 1.58 ± 0.35 eV for the $HfSiO_4$/β-Ga_2O_3 system using the differences in bandgaps and the directly measured valence band offset, ie.: $\Delta E_C = E_g^{HfSiO_4} - E_g^{AlGaO} - \Delta E_V$, ie. $\Delta E_C = 7.0\ eV - 5.0\ eV - 0.42\ eV = 1.58$ eV. The valence band offset is below the desirable 1 eV magnitude, but the conduction band offset is well above this value, ensuring good electron confinement, especially for high-temperature device operation.

Currently, there are no other measurements of the band offsets of $HfSiO_4$ on $(Al_xGa_{1-x})_2O_3$. We measured a valence offset for ALD SiO_2 on β-$(Al_{0.14}Ga_{0.86})_2O_3$ of 1.60 eV ± 0.40 eV (straddling gap, type I alignment). The conduction band offset was 2.10 ± 0.08 eV.[23] These values are in agreeance with ALD SiO_2 band offset values determined in previous studies. There is a strong influence of factors such as the variation in bandgap of the dielectrics due to differences in measurement protocols and stoichiometry resulting from different deposition methods, chemistry and contamination. There are also influences of strain, defects/vacancies, stoichiometry, chemical bonding and contamination on valence band offset values AGO/dielectric heterojunctions. As an example, dielectrics deposited by sputtering will have a higher likelihood of interfacial disorder and metallic contamination that affects the bandgap of the dielectric.[38–42]

Conclusions

The band alignment at $HfSiO_4$/ β-$(Al_{0.14}Ga_{0.86})_2O_3$ heterojunctions is a nested gap (type I) band offset. The valence band offset was 0.42 ± 0.10 eV and the conduction band offset was 1.58 ± 0.35 eV. The conduction band offset is large and provides excellent electron confinement, while the valence band offset would be marginal for restricting hole transport. At this point, p-type conduction in Ga_2O_3 and $(Al_xGa_{1-x})_2O_3$ is unachievable using conventional dopants,[49,50] so the electron confinement by the conduction band offset is most important.

Acknowledgments

The project or effort depicted was partially sponsored by the Department of the Defense, Defense Threat Reduction Agency, HDTRA1-17-1-011, monitored by Jacob Calkins. The content of the information does not necessarily reflect the position or the policy of the federal government, and no official endorsement should be inferred.

ORCID

Chaker Fares https://orcid.org/0000-0001-9596-2381
F. Ren https://orcid.org/0000-0001-9234-019X

Downloaded on 2018-10-30 to IP 128.227.118.70 address. Redistribution subject to ECS terms of use (see ecsdl.org/site/terms_use) unless CC License in place (see abstract).

S. J. Pearton https://orcid.org/0000-0001-6498-1256

References

1. M. J. Tadjer, N. A. Mahadik, J. A. Freitas, E. R. Glaser, A. D. Koehler, L. E. Luna, B. N. Feigelson, K. D. Hobart, F. J. Kub, and A. Kuramata, Ga_2O_3 Schottky barrier and heterojunction diodes for power electronics applications, *Proc. SPIE 10532, GaN Materials and Devices XII*I, 1053212 (2018).
2. Burhan Bayraktaroglu, Assessment of Gallium Oxide Technology,Devices for Sensing Branch Aerospace Components & Subsystems Division, AFRL-RY-WP-TR-2017-0167, August 2017, http://www.dtic.mil/dtic/tr/fulltext/u2/1038137.pdf
3. Serdal Okur, Gary S. Tompa, Nick Sbrockey, Tom Salagaj, Volker Blank, Bernd Henninger, Michele Baldini, Günter Wagner, Zbigniew Galazka, Yao Yao, J. Rokholt, Robert F. Davis, Lisa M. Porter, and Abraham Belkind, Vacuum Technology and Coating, May 2017, pp.31
4. S. J. Pearton, Jiancheng Yang, Patrick H. Cary IV, F. Ren, Jihyun Kim, Marko J. Tadjer, and Michael A. Mastro, *App. Phys. Rev.*, **5**, 011301 (2018).
5. Masataka Higashiwaki and Gregg H. Jessen, *Appl. Phys. Lett.*, **112**, 060401 (2018).
6. Masataka Higashiwaki, Kohei Sasaki, Hisashi Murakami, Yoshinao Kumagai, Akinori Koukitu, Akito Kuramata, Takekazu Masui, and Shigenobu Yamakosh, *Semicond. Sci. Technol.*, **31**, 034001 (2016).
7. Joe F. McGlone, Zhanbo Xia, Yuewei Zhang, Chandan Joishi, Saurabh Lodha, Siddharth Rajan, Steven A. Ringel, Aaron, and R. Arehart, *IEEE Electron Device Letters*, **39**, 1042 (2018).
8. S. Oh, J. Kim, Fan Ren, S. J. Pearton, and Jihyun Kim, *J. Mater. Chem. C*, **4**, 9245 (2016).
9. Kelson D. Chabak, Neil Moser, Andrew J. Green, Dennis E. Walker Jr., Stephen E. Tetlak, Eric Heller, Antonio Crespo, Robert Fitch, Jonathan P. McCandless, Kevin Leedy, Michele Baldini, Gunter Wagner, Zbigniew Galazka, Xiuling Li, and Gregg Jessen, *Appl. Phys. Lett.*, **109**, 213501 (2016).
10. Andrew J. Green, Kelson D. Chabak, Eric R. Heller, Robert C. Fitch Jr., Michele Baldini, Andreas Fiedler, Klaus Irmscher, Günter Wagner, Zbigniew Galazka, Stephen E. Tetlak, Antonio Crespo, Kevin Leedy, and Gregg H. Jessen, *IEEE Electron Dev. Lett.*, **37**, 902 (2016).
11. M. J. Tadjer, N. A. Mahadik, V. D. Wheeler, E. R. Glaser, L. Ruppalt, A. D. Koehler, K. D. Hobart, C. R. Eddy Jr., and F. J. Kub, *ECS J. Solid State Sci. Technol.*, **5**, 468 (2016).
12. K. D. Chabak, J. P. McCandless, N. A. Moser, A. J. Green, K. Mahalingam, A. Crespo, N. Hendricks, B. B. Howe, S. E. Tetlak, K. Leedy, R. C. Fitch, D. Wakimoto, K. Sasaki, A. Kuramata, and G. H. Jessen, *IEEE Electron Device Lett*. **39**, 67 (2018).
13. K. Konishi, K. Goto, H. Murakami, Y. Kumagai, A. Kuramata, S. Yamakoshi, and M. Higashiwaki, *Appl. Phys. Lett.*, **110**, 103506 (2017).
14. Janghyuk Kim, Sooyeoun Oh, Michael Mastro, and Jihyun Kim, *Phys. Chem. Chem Phys.*, **18**, 15760 (2016).
15. Y. Zhang, A. Neal, Zhanbo Xia, C. Joishi, J. M. Johnson, Y. Zheng, S. Bajaj, M. Brenner, D. Dorsey, K. Chabak, G. Jessen, J. Hwang, Shin Mou, J. P. Heremans, and S. Rajan, *Appl. Phys. Lett.*, **112**, 173502 (2018).
16. S. Krishnamoorthy, Z. Xia, C. Joishi, Y. Zhang, J. McGlone, J. Johnson, M. Brenner, A. R. Arehart, J. Hwang, and S. Lodha, *Appl. Phys. Lett.*, **111**, 023502 (2017).
17. E. Ahmadi, O. S. Koksaldi, X. Zheng, T. Mates, Y. Oshima, U. K. Mishra, and J. S. Speck, *Appl. Phys. Express*, **10**, 071101 (2017).
18. T. Oshima, Y. Kato, N. Kawano, A. Kuramata, S. Yamakoshi, S. Fujita, T. Oishi, and M. Kasu, *Appl. Phys. Express*, **10**(3), 035701 (2017).
19. Yuewei Zhang, Chandan Joishi, Zhanbo Xia, Mark Brenner, Saurabh Lodha, and Siddharth Rajan, *Appl. Phys. Lett.*, **112**, 233503 (2018).
20. Fabi Zhang, Katsuhiko Saito, Tooru Tanaka, Mitsuhiro Nishio, Makoto Arita, and Qixin Guo, *Appl. Phys. Lett.*, **105**, 162107 (2014).
21. Ryo Wakabayashi, Mai Hattori, Kohei Yoshimatsu, Koji Horiba, Hiroshi Kumigashira, and Akira Ohtomo, *Appl. Phys. Lett.*, **112**, 232103 (2018).
22. Hartwin Peelaers, Joel B. Varley, James S. Speck, and Chris G. Van de Walle, *Appl. Phys. Lett.*, **112**, 242101 (2018).
23. Zhaoqing Feng, Qian Feng, Jincheng Zhang, Xiang Li, Fuguo Li, Lu Huang, Hong-Yan Chen, Hong-Liang Lu, and Yue Hao, *Appl. Surf. Sci.*, **434**, 440 (2018).
24. Y. Jia, K. Zheng, J. S. Wallace, J. A. Gardella, and U. Singisetti, *Appl. Phys. Lett.*, **106**, 102107 (2016).
25. K. Konishi, T. Kamimura, M. H. Wong, K. Sasaki, A. Kuramata, S. Yamakoshi, and M. Higashiwaki, *Phys. Status Solidi B*, **253**, 623 (2016).
26. T. Kamimura, K. Sasaki, M. H. Wong, D. Krishnamurthy, A. Kuramata, T. Masui, S. Yamakoshi, and M. Higashiwaki, *Appl. Phys. Lett.*, **104**, 192104 (2014).
27. M. Hattori, T. Oshima, R. Wakabayashi, K. Yoshimatsu, K. Sasaki, T. Masui, A. Kuramata, S. Yamakoshi, K. Horiba, H. Kumigashira, and A. Ohtomo, *Jpn. J. Appl. Phys.*, **55**, 1202B6 (2016).
28. Virginia D. Wheeler, David I. Shahin, Marko J. Tadjer, and Charles R. Eddy Jr., *ECS J. Solid State Sci. Technol.*, **6**, Q3052 (2017).
29. W. Wei, Z. Qin, S. Fan, Z. Li, K. Shi, Q. Zhu, and G. Zhang, *Nanoscale Res. Lett*, **7**, 562 (2012).
30. S. H. Chang, Z. Z. Chen, W. Huang, X. C. Liu, B. Y. Chen, Z. Z. Li, and E. W. Shi, *Chin. Phys. B.*, **20**, 116101 (2011).
31. Z. Chen, K. Hishihagi, X. Wang, K. Saito, T. Tanaka, M. Nishio, M. Arita, and Q. Guo, *Appl. Phys. Lett.*, **109**, 102106 (2016).
32. P. H. Carey, F. Ren, D. C. Hays, B. P. Gila, S. J. Pearton, S. Jang, and A. Kuramata, *J. Vac. Sci. Technol. B.*, **35**, 041201 (2017).
33. P. Carey, F. Ren, D. C. Hays, B. P. Gila, S. J. Pearton, S. Jang, and A. Kuramata, *Jpn. J. Appl. Phys.*, **56**, 071101 (2017).
34. P. Carey, F. Ren, D. C. Hays, B. P. Gila, S. J. Pearton, S. Jang, and A. Kuramata, *Vacuum*, **142**, 52 (2017).
35. David C. Hays, B. P. Gila, S. J. Pearton, Andres Trucco, Ryan Thorpe, and F. Ren, *J. Vac. Sci. Technol. B.*, **35**, 011206 (2017).
36. D. C. Hays, B. P. Gila, S. J. Pearton, and F. Ren, *Appl. Phys. Rev.*, **4**, 021301 (2017).
37. E. A. Kraut, R. W. Grant, J. R. Waldrop, and S. P. Kowalczyk, *Phys. Rev. Lett.*, **44**, 1620 (1980).
38. E. Bersch, M. Di, S. Consiglio, R. D. Clark, G. J. Leusink, and A. C. Diebold, *J. Appl. Phys.*, **107**, 043702 (2010).
39. H. C. Shin, D. Tahir, S. Seo, Y. R. Denny, S. K. Oh, H. J. Kang, S. Heo, J. G. Chung, J. C. Lee, and S. Tougaard, *Surf. Interface Anal.*, **44**, 623 (2012).
40. A. Klein, *J. Phys. C. Solid*, **27**, 134201 (2015).
41. J. Robertson and S. J. Clark, *Phys. Rev. B*, **83**, 075205 (2011).
42. F. Chen, R. Schafranek, S. Li, W. Wu, and A. J. Klein, *J. Phys. D*, **43**, 295301 (2010).
43. S. Li, F. Chen, R. Schafranek, T. J. M. Bayer, K. Rachut, A. Fuchs, S. Siol, M. Weidner, M. Hohmann, V. Pfeifer, J. Morasch, C Ghinea, E. Arveux, R. Gunzler, J. Gassmann, C. Korber, Y. Gassenbauer, F. Sauberlich, G. V. Rao, S. Payan, M. Maglione, C. Chirila, L. Pintilie, L. Jia, K. Ellmer, M. Naderer, K. Reichmann, U. Bottger, S. Schmelzer, R. C. Frunza, H. Ursic, B. Malic, W.-B. Wu, P. Erhart, and A. Klein, *Phys Status Solidi Rapid Res Let*. **8**, 571 (2014).
44. A. Klein, *Thin Solid Films*, **520**, 3721 (2012).
45. Chris G. Van de Walle and L. H. Yang, *J. Vac. Sci. Technol. B*, **13**, 1635 (1995).
46. X. Guo, H. Zheng, S. W. King, V. V. Afanas'ev, M. R. Baklanov, J.-F. D. Marneffe, Y. Nishi, and J. L. Shohet, *Appl. Phys. Lett.*, **107**, 082903 (2015).
47. J. Xu, Y. Teng, and F. Teng, *Scientific Reports*, **6**, 32457 (2016).
48. Benjamin W. Krueger, Christopher S. Dandeneau, Evan M. Nelson, Scott T. Dunham, Fumio S. Ohuchi, and Marjorie A. Olmstead, *J. Am. Ceram. Soc.*, **99**, 2467 (2016).
49. Alexandros Kyrtsos, Masahiko Matsubara, and Enrico Bellotti, *Appl. Phys. Lett.*, **112**, 032108 (2018).
50. Ekaterine Chikoidze, Adel Fellous, Amador Perez-Tomas, Guillaume Sauthier, Tamar Tchelidze, Cuong Ton-That, Tung Thanh Huynh, Matthew Phillips, Stephen Russell, Mike Jennings, Bruno Berini, Francois Jomard, and Yves Dumont, *Mat. Today Phys*. **3**, 118 (2017).

Downloaded on 2018-10-30 to IP 128.227.118.70 address. Redistribution subject to ECS terms of use (see ecsdl.org/site/terms_use) unless CC License in place (see abstract).